Hypermodified Nucleosides in the Anticodon of tRNA^{Lys} Stabilize a Canonical U-Turn Structure[†,‡]

Mallikarjun Sundaram,[§] Philippe C. Durant, and Darrell R. Davis*

Department of Medicinal Chemistry, University of Utah, Salt Lake City, Utah 84112, USA

Received June 27, 2000; Revised Manuscript Received August 9, 2000

ABSTRACT: Modified nucleosides in the anticodon domain of *Escherichia coli* tRNA^{Lys} are necessary for high-affinity codon recognition and reading frame maintenance. Human tRNA^{Lys,3} is the specific primer for HIV-1 reverse transcriptase and also requires nucleoside modification for proper function. We now present NMR solution structures for the fully modified 17-nucleotide *E. coli* tRNA^{Lys} anticodon stem-loop domain (ASL). NMR data were also collected for several partially modified ASLs, revealing the contributions each modified nucleoside (mnm^{5}s^{2}U34, t^{6}A37, and ψ39) makes in transforming the disordered, unmodified tRNA ASL into the highly ordered native structure. The solution structure of the native ASL domain provides insight into longstanding questions regarding both wobble position modification and the nearly ubiquitous t^{6}A37 found in tRNAs with an adjacent U at position 36. Native tRNA^{Lys} has a U-turn structure similar to the yeast tRNA^{Phe} crystal structure, unlike previously proposed "unconventional" anticodon structures characterized by stable interactions between mnm^{5}s^{2}U-34 and t^{6}A-37.

Human tRNA^{Lys,3} and the single tRNA^{Lys} isoacceptor in *Escherichia coli* both have the anticodon sequence $U_{34}U_{35}U_{36}$, and the anticodon domains are highly functionalized with hypermodified nucleosides at positions 34 and 37 (Figure 1). The requirement for hypermodification is underscored by results that show that the unmodified anticodon is relatively unstructured (*1*) and that nucleoside modification is necessary for mRNA-dependent ribosome binding (*2*, *3*). The tRNA anticodon is a specific recognition element for lysyl tRNA synthetase, with the anticodon nucleoside modifications providing a 140-fold increase in binding affinity over an unmodified tRNA transcript (*4*). Similarly, in the human immunodeficiency virus 1 (HIV-1)[1] transcription initiation complex, there is a modification-dependent interaction between the anticodon of tRNA^{Lys,3} and the HIV genomic RNA (*5*, *6*), and there is also an interaction between the tRNA^{Lys,3} anticodon and reverse transcriptase (RT) (*7*−*9*). Biochemical studies have implicated the hypermodified 5-methylcarboxymethyl,2-thiouridine (mcm^{5}s^{2}U) nucleoside as the main contributor to stabilization of the complex between the tRNA anticodon and the HIV A-rich loop (*10*, *11*). The very similar modifications in human tRNA^{Lys,3} and *E. coli* tRNA^{Lys} suggest that *E. coli* tRNA^{Lys} will also be a good structural model for the anticodon of human tRNA^{Lys,3}, and the *E. coli* tRNA^{Lys} structure should give insights into the effects nucleoside modifications have on tRNA interactions with HIV-1 genomic RNA and with HIV-1 RT.

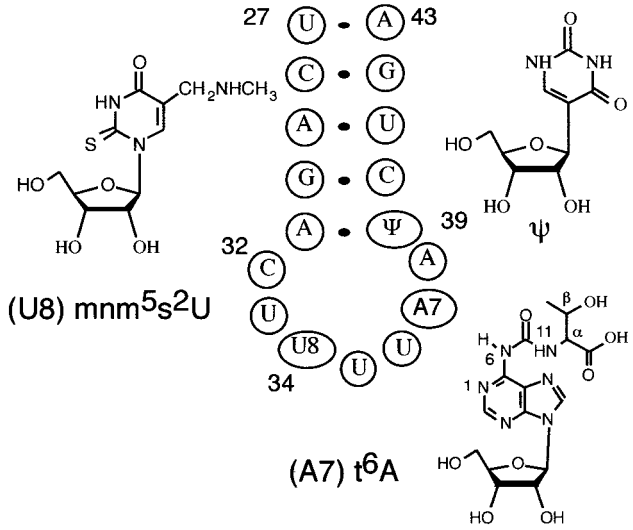

FIGURE 1: RNA secondary structure and structures of the modified bases for the *E. coli* tRNA^{Lys} ASL. The upper stem sequence of human tRNA^{Lys,3} was used to facilitate subsequent comparisons between the human and the *E. coli* isoacceptors. The two tRNAs have the same sequence for the last two base-pairs and the loop, the "extended anticodon". Human tRNA^{Lys,3} has mcm^{5}s^{2}U34, ms^{2}t^{6}A37, and ψ39 modifications in the anticodon domain. In the text, native tRNA^{Lys} refers to the fully modified ASL with mnm^{5}s^2-U34, t^{6}A37, and ψ39. Doubly modified ASLs contain either U34 or A37.

[†] The work was supported by National Institutes of Health Grant GM55508 to D.R.D., by Grants RR06262 and RR13030 for NMR instruments, and by Grant CA42014 to support the RNA synthesis and mass spectrometry facilities.

[‡] The coordinates have been deposited with the Protein Data Bank under accession code 1FL8.

* To whom correspondence should be addressed. Darrell R. Davis, Department of Medicinal Chemistry, University of Utah, 30 S. 2000 E. Room 307, Salt Lake City, UT 84112-5820, (801) 581-7006, E-mail: davis@adenosine.pharm.utah.edu.

[§] Present address: Department of Bioengineering and Environmental Health, Massachusetts Institute of Technology, Cambridge, MA 02139.

[1] Abbreviations: ASL, anticodon stem-loop; HIV-1, human immunodeficiency virus 1; RT, reverse transcriptase; ψ, pseudouridine; mnm^{5}s^{2}U, 5-methylaminomethyl,2-thiouridine; mcm^{5}s^{2}U, 5-methylcarboxymethyl,2-thiouridine; s^{4}U, 4-thiouridine; t^{6}A, *N*-[(9-β-D-ribofuranosyl-9H-purin-6-yl)carbamoyl])-l-threonine; NOE, nuclear Overhauser effect; MALDI-MS, matrix assisted laser desorption ionization mass spectrometry; LC/MS, liquid chromatography/mass spectrometry; NOESY, nuclear Overhauser effect spectroscopy; COSY, correlation spectroscopy; TOCSY, total correlation spectroscopy.

10.1021/bi0014655 CCC: $19.00
Published on Web 09/19/2000

$tRNA^{Lys}$ exhibits high frameshifting frequencies at A−AAA−AAG mRNA sites where the A-site tRNA initially has the wobble position nucleotide paired with G and then slips 1 nucleotide in the 5′ direction to pair with an evidently more stable AAA codon (*12*, *13*). In the example from the *dnaX* gene with tandem lysine codons, the P-site tRNA appears to simultaneously move in the 5′ direction along with the A-site tRNA where the 5′ A allows for two AAA codons in the −1 frame. The "shiftiness" of $tRNA^{Lys}$ in the A-site is also seen with other codons in the P-site, as seen for the *Bacillus subtilis* cytidine deaminase gene frameshift site (CGA−AAG), where a −1 frameshift of A-site $tRNA^{Lys}$ occurs with $tRNA^{Arg}$ in the P-site (*14*). Hagervall and coworkers have investigated lysine tRNA facilitated frameshifting in modification deficient *E. coli* mutants to delineate the effects individual functional groups of the 5-methylaminomethyl,2-thiouridine (mnm^5s^2U) nucleoside have on frameshifting. While the frameshifting frequencies are sensitive to the modification status of the wobble nucleoside, no conclusive model was apparent from their results (*15*). Wobble modification in $tRNA^{Lys}$ also affects in-frame codon−anticodon recognition as shown by the misreading of asparagine codons (AAU/C) by $tRNA^{Lys}$ during asparagine starvation (*16*).

Unconventional structures have been proposed to explain the unusual functional properties of $tRNA^{Lys}$ (*17*, *18*), and NMR studies of a pentamer model for the anticodon led to a proposed structure in which the key feature was a direct interaction between mnm^5s^2U34 and t^6A (*18*). The 17-nucleotide $tRNA^{Lys}$ ASL in Figure 1 is structurally restrained as compared to the pentamer model studied previously, and the hairpin restraint may prevent non-native interactions between the highly functionalized modified nucleosides. tRNA ASLs have been shown to be functionally competent in mRNA dependent ribosome binding (*2*, *3*, *19*) and represent a minimal system for structure determination of the anticodon domain. We had previously determined the structure of the unmodified $tRNA^{Lys}$ ASL and the ASL with a single pseudouridine (ψ) modification (*1*). These structures were quite dynamic and allowed for a noncanonical A^+−C interaction at the base of the stem. The major questions of the current study were whether the introduction of the hypermodified nucleosides would significantly restrict the conformational flexibility of the 7-nucleotide anticodon loop, whether the native ASL adopts a structure similar to other well-characterized tRNAs, and whether there are direct contacts between the hypermodified nucleosides. Resolving these issues is critical for understanding the unique properties of $tRNA^{Lys}$ and for understanding structure−function properties of these hypermodified nucleosides in other tRNA isoacceptors.

MATERIALS AND METHODS

RNA Synthesis and Purification. RNA oligonucleotides were synthesized on a 1-μmol scale using PAC phophoramidites (Glen Research). The modified phosphoramidites were synthesized and incorporated into the $tRNA^{Lys}$ ASLs as we have described (*20*). The normal I_2/H_2O oxidation solution was used until the mnm^5s^2U nucleoside was added, and 2 × 5 min oxidation cycles with 10% tBuOOH in acetonitrile were used subsequently. The RNA was deprotected using a multistep protocol specifically optimized for the functional groups on the hypermodified nucleosides. The column bound material was treated with 10% *tert*-butylamine in dry pyridine, and the support material was then dried to remove acrylonitrile. The RNA was then cleaved from the column, and the base protecting groups were removed with NH_4OH/ethanol (3:1, v/v). The solution was lyophilized and then subjected to a two-step fluoride treatment with neat $Et_3N{\cdot}3HF$ followed by tetrabutylammonium fluoride in tetrahydrofuran (*21*, *22*). Two different fluoride reagents were required to cleanly remove the trimethylsilylethyl group used to protect the t^6A carboxylate and to remove the *tert*-butyldimethylsilyl groups on the sugars and the t^6A secondary hydroxyl. The tetrabutylammonium fluoride solution was dried to a viscous gum and redissolved in water, and the solution was passed through an NAP-25 (Pharmacia) column to remove the excess tetrabutylammonium ions. The RNA was then purified by anion exchange HPLC using a Resource Q (Pharmacia) column (*23*).

Mass Spectrometry. The compositions of the crude RNAs and the final, purified RNAs were determined by molecular weight measurements using MALDI-MS as described (*20*). The presence of specific modified nucleosides was determined by liquid chromatography/mass spectrometry (LC/MS) (*24*) using a HP 1090 liquid chromatograph interfaced to a Fisons Quattro II triple quadrupole mass spectrometer (Manchester, UK) using electrospray ionization. Nucleoside samples for LC/MS were prepared by digesting approximately 50 μg each of the native tRNA, oxidized native tRNA, and the native tRNA ASL to mononucleosides using nuclease P1, phosphodiesterase I, and then alkaline phosphatase (*25*).

CD Spectroscopy and UV Spectroscopy. CD spectroscopy was done on 1.5−3.0 μM RNA samples in the NMR buffer using a JASCO 720 spectrometer with 1-cm temperature regulated CD cells. The RNA concentrations were determined by UV absorption assuming an extinction coefficient of 1.73×10^5 L mol^{-1} cm^{-1}. Ellipticities are reported per mole of RNA oligonucleotide. The full-length, native *E. coli* $tRNA^{Lys}$ (Sigma) was selectively oxidized using 10% tBuOOH in acetonitrile while monitoring the change in ellipticity at 330 nm (∼60 min). UV absorbance vs temperature (T_m) measurements were done on an HP 8452A spectrophotometer; the temperature was increased in 1 °C increments with a 1-min equilibration time. Melting experiment samples contained 10 μM RNA dissolved in NMR buffer. Measurements were repeated four times for each hairpin, and the T_m and thermodynamic parameters were calculated with the Melt Fit II program assuming a two-state transition (*26*).

NMR Data Acquisition and Analysis. RNA samples were dissolved in 10 mM phosphate buffer at pH 7.0 containing 50 mM KCl, 50 mM NaCl, and either 0 or 10 mM $MgCl_2$ to final RNA concentrations of 1.5 mM. NMR data was collected on Varian Unity 500 and Varian INOVA 600 NMR spectrometers using Nalorac probes. The fully modified and partially modified hairpins were monomers at NMR concentrations as determined by measuring their translational diffusion rates (*27*) and by measuring T_m's over a 100-fold concentration range from 2 to 200 μM. The NMR spectra were assigned using 2D NOESY (*28*) and TOCSY (*29*) NMR experiments following the basic sequential assignment strategy established for RNA (*30*). Complete assignments were made for all nonexchangeable protons, except that stereospecific assignments were not made for the H5′/H5″

protons. The imino protons were assigned from 2D NOESY spectra at 10 °C in 90% H_2O buffer using a NOESY pulse sequence with a flip-back WATERGATE element (*31*). The ^{31}P spectra were assigned using a combination of 2D heteronuclear COSY (*32*) and 2D hetero-TOCSY-TOCSY (*33*) experiments. DQCOSY (*34*) was used for sugar coupling constant measurements. Data were processed and analyzed with VNMR (Varian) and Felix (MSI) software. Unambiguous assignments were facilitated by comparing the 2D NOESY spectra for the native tRNA^{Lys} ASL and three different doubly modified tRNA^{Lys} ASLs: tRNA^{Lys}-mnm^{5}s^2-U34, ψ39; tRNA^{Lys}-t^{6}A37, ψ39; and tRNA^{Lys}-s^{2}U34, ψ39 (Supporting Information).

Restraint Determination. Distance restraints were determined from 2D NOESY data in water and in D_2O collected with a 180 ms mixing time. An upper bound was determined for a small number of proton pairs based on NOEs observed in 400 ms NOESY spectra. Restraints were only included from the 400 ms data in cases where spin diffusion could clearly be ruled out. Nuclear Overhauser effect (NOE) volumes were converted to distances by scaling to the H5−H6 cross-peaks of uridine and cytidine. The sugars were restrained to the 3′-endo conformation in cases where there was no detectable H1′-H2′ DQCOSY or TOCSY cross-peak. Residues 33−36 all had some percentage of 2′-endo character based on the correlation experiments, and the sugars were left unrestrained. The backbone α and ζ angles were restrained based on the ^{31}P chemical shifts according to the method of Moore and co-workers (*35*). This method essentially restrains phosphates with chemical shifts in the A-form range to A-RNA geometries and leaves phosphates with anomalous shifts unrestrained. The nucleosides with "unusual" phosphates were given additional conformational freedom during the refinement by also using loose backbone restraints for their 5′ and 3′ neighbors, and the remaining loop residues were given a wider range within the allowed conformations than the stem residues.

The five stem base pairs were maintained using hydrogen-bonding restraints set to 1.8 ± 0.2 Å for the central base pairs and 2.1 ± 0.3 Å for the weaker base pairs at the ends of the stem. Restraints for the A−U base pairs also included adenosine H2 to uridine O2 restraints to maintain base pair planarity. Dihedral angles for the stem residues were restrained to literature A-RNA values ± 30° (α, β, γ, ϵ, ζ). Ribose sugar dihedrals for stem residues and the 100% 3′-endo loop residues were set to A-RNA values ± 20°. Ribose dihedral angles for loop residues that were not 100% 3′-endo (residues 33−36) were not restrained. Except for special cases discussed below, loop residue dihedral angles (α, β, γ, ϵ, ζ) were allowed to encompass A- and B-form values ± 30°. To accommodate the downfield shifted phosphate assigned to 33p34, the α and ζ angles for 34 were not restrained. The α and ζ angles were also left unrestrained for mnm^{5}s^{2}U34 and ψ39 because strong P−H4′ cross-peaks for these residues were seen in the ^{1}H-^{31}P heteronuclear COSY spectrum. All χ dihedral angles were restrained to the anti range ± 90°.

Structure Determination. Structure calculations were performed using the general strategy we described previously (*1*) and detailed below (Table 1). Molecular dynamics calculations were done with the NMR Refine module of the Insight/Discover program (MSI) and the AMBER force field (*36*). The initial phase of the restrained molecular dynamics simulations included 3.5 ps of restrained dynamics at 1200 K with initial force constants scaled by 0.01 (distance) and 0.05 (dihedral). In the final 2 ps of this 1200 K period, the scale factor was increased in two steps to final values of 0.04 (distance) and 0.2 (dihedral). A subsequent 3 ps of dynamics at 1200 K started with relaxation of the scale factor to 0.01 (distance) and 0.025 (dihedral) for 1 ps and then a two-step increase as before to final values of 1.0 (distance) and 0.1 (dihedral). After this 1200 K equilibration run, the temperature was first cooled to 850 K and then to 100 K in 5 × 1 ps steps with scale factors of 0.75 (distance) and 0.05 (dihedral). The final step of the refinement involved conjugate gradient energy minimization until a maximum derivative of less than 0.05 was obtained. The scale factors were set to 0.015 (distance) and 0.005 (dihedral) during the energy minimization. To avoid having the base pairs fall apart and to prevent the loop from expanding during the weakly restrained minimization, the force constants for the base pair restraints were increased, and the U33 N3H and U36 O1P atoms were fixed.

RESULTS

CD spectroscopy of Native tRNA^{Lys} and Native tRNA^{Lys} ASL. Sulfur-modified uridine nucleosides have a long wavelength UV absorption with a maximum near 330 nm, and this contributes a band in the CD spectrum that is sensitive to local RNA structure (*17*, *37*−*39*). The sign and intensity of the sulfur CD band can be used to monitor structural stability and even to probe base pairing interactions. CD spectroscopy was used to provide a qualitative measurement of the secondary structure of the tRNA^{Lys} ASLs and to compare the synthetic ASLs with full-length, native *E. coli* tRNA^{Lys}. The CD spectra in the region of the UV absorbance maximum displayed typical A-RNA like behavior (not shown) with the major band near 260 nm decreasing in intensity with increasing temperature. The long wavelength region of the CD spectra of our native tRNA^{Lys} ASL is shown in Figure 2, trace c. The negative ellipticity with a maximum at 338 nm is typical of thiolated uridines in single-stranded structural environments (*17*). This indicates that the mnm^{5}s^{2}U nucleoside does not form a stable base-pairing type interaction with other nucleosides in the tRNA anticodon. The negative ellipticity for the ASL is in contrast to the positive band for the full-length native tRNA in Figure 2, trace a. The CD spectrum in Figure 2, trace a is very similar to that reported previously and was given as evidence for a stable interaction involving mnm^{5}s^{2}U (*17*). However, *E. coli* tRNA^{Lys} contains 4-thiouridine (s^{4}U) at position 8 in addition to mnm^{5}s^{2}U34. The positive CD band at 330 nm is very characteristic of the s^{4}U8 nucleoside in tRNA (*37*), which forms the highly conserved reversed-Hoogsteen tertiary base pair with A14 (*40*, *41*). Since the tRNA^{Lys} CD spectrum contained contributions from both s^{4}U8 and mnm^{5}s^{2}U34, we selectively oxidized the s^{4}U in full-length tRNA^{Lys} and obtained the CD spectrum shown in Figure 2, trace b where the only contribution to the long wavelength ellipticity is from mnm^{5}s^{2}U. The nucleoside compositions of each tRNA sample in Figure 2 were verified by enzymatically digesting the tRNAs and the ASL to mononucleosides and then analyzing the nucleoside mixtures by LC/MS (*24*). The presence of s^{4}U, mnm^{5}s^{2}U, and t^{6}A was confirmed for the

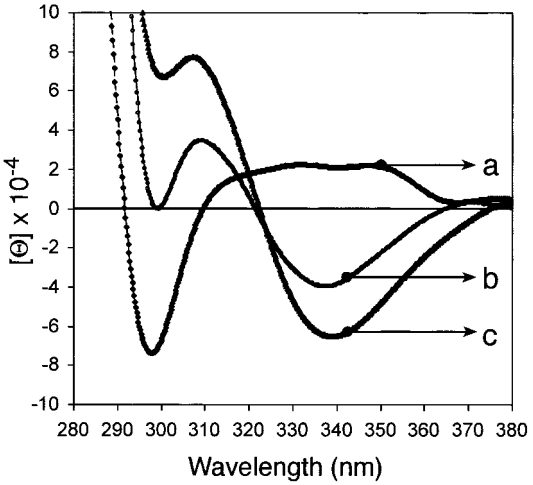

FIGURE 2: CD spectra of (a) native tRNA^{Lys} (1.5 μM); (b) native tRNA^{Lys} after selective oxidation of s^{4}U8; (c) the tRNA^{Lys} 17-mer ASL (3.0 μM) for the long-wavelength region where the ellipticity is due to thiouridine nucleosides. The negative ellipticity due to mnm^{5}s^{2}U34 in trace b is no longer masked by the more intense contribution from s^{4}U8 in trace a. The CD spectra indicate that the ASL structure is similar to the native tRNA and to *E. coli* tRNA^{Glu} which does not have t^{6}A or s^{4}U8 (*17*).

commercial *E. coli* tRNA^{Lys}, while the selectively oxidized tRNA was missing s^{4}U. The composition of the native tRNA^{Lys}ASL was confirmed by LC/MS analysis of the digested oligonucleotide and by MALDI-MS of the intact RNA (*20*).

Exchangeable Proton Spectra. Imino spectra at 10 °C of the native tRNA^{Lys} and the doubly modified tRNA^{Lys}-mnm^{5}s^{2}U34,ψ39 and tRNA^{Lys}-t^{6}A37,ψ39 hairpins are shown in Figure 3. The tRNA^{Lys}-mnm^{5}s^{2}U34,ψ39 hairpin (Figure 3, trace c) has the simplest NMR spectrum since the wobble modification contributes no additional resonances to the downfield region. Peaks are seen for the three central Watson−Crick base pairs and for the A31-ψ39 interaction at the base of the stem. Pseudouridine stabilizes the T_m by nearly 5 °C, and this stabilization of the 31−39 base pair is required to slow the imino exchange sufficiently to observe an N3−H resonance. We have not been able to detect an imino proton resonance for the A31-U39 interaction in tRNA^{Lys} ASLs with unmodified U39. In addition to the ψ39N3-H proton hydrogen bonded to A31, the ψ39N1-H proton coordinated to a stable water molecule is seen at 10.7 ppm.

The native tRNA^{Lys} imino spectrum (Figure 3, trace a) contains several additional peaks as a result of t^{6}A37. The amide proton resonances at 9.0 and 10.2 ppm were assigned from 2D NOESY and TOCSY connectivities. The NH11 resonance has TOCSY connectivity to the Hα and Hβ resonances of the side chain as well as NOE connectivity to side chain protons as discussed below. The sharp resonance at 8.6 ppm is the t^{6}A H2 proton. Another additional weak imino resonance is seen at 11.3 ppm in the native tRNA^{Lys} spectrum and a similar resonance at 11.5 ppm in the tRNA^{Lys}-t^{6}A37,ψ39 spectrum is seen in Figure 3, trace b. This peak is due to the U33 N3-H imino proton hydrogen bonded to the phosphate between U35 and U36. The support for this assignment is indirect but seems compelling. First, there are a limited number of possible residues that could contribute an imino resonance at this position, namely, the loop uridines.

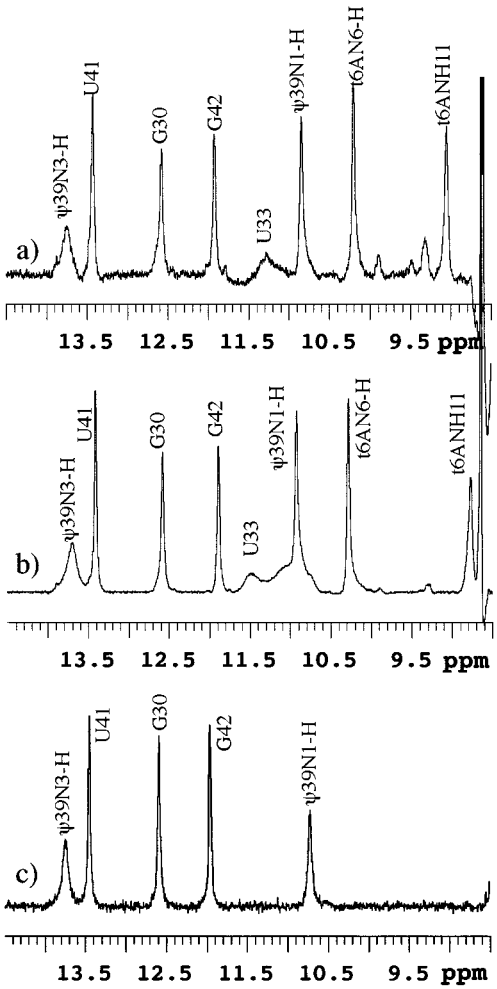

FIGURE 3: (a) Imino spectra for the native tRNA^{Lys} ASL, 10 °C. The ^{1}H NMR spectrum of the exchangeable imino protons indicate stable hydrogen bonding interactions for the three central Watson−Crick base pairs and for the A31-ψ39 interaction at the base of the stem. NMR resonances are seen for ψ39 N3-H and the characteristic ψN1-H proton hydrogen-bonded through a water molecule to the phosphates of A38 and ψ39. The two peaks for the amide protons of t^{6}A are upfield of the ψ N1-H resonance. A weak resonance is seen at 11.3 ppm, which is assigned to the U33 imino proton. (b) Imino spectra for the tRNA^{Lys}-t^{6}A37, ψ39 ASL, 10 °C. (c) Imino spectra for the tRNA^{Lys}-mnm^{5}s^{2}U34, ψ39 ASL, 10 °C.

The chemical shift is characteristic of a uridine hydrogen bonded to a phosphate (*42*) and is nearly identical to that seen for an ASL of yeast tRNA^{Phe} (*43*). We have also seen a similar, though more stable resonance for a tRNA^{Leu} ASL hairpin and unambiguously assigned this resonance by specific ^{15}N labeling (unpublished).

Phosphorus NMR. The ^{31}P NMR spectrum of the native tRNA^{Lys} ASL has a single phosphorus resonance shifted significantly downfield of the envelope of resonances (*20*). This resonance was assigned to the 33p34 phosphate using 2D ^{1}H-^{31}P COSY and ^{1}H-^{31}P hetero-TOCSY-TOCSY experiments. The significant shift in the ^{31}P NMR spectrum indicates either the α or ζ angle is trans, consistent with a π-turn geometry in the tRNA ASL (*44*, *45*). We also observed a downfield shifted 33p34 phosphorus resonance (Supporting Information) for tRNA^{Lys}-mnm^{5}s^{2}U34,ψ39, indicating the backbone angle is also trans in the doubly modified ASL. In contrast, we saw no such NMR resonance for tRNA^{Lys}-s^{2}U34,ψ39 or tRNA^{Lys}-t^{6}A37,ψ39 indicating that

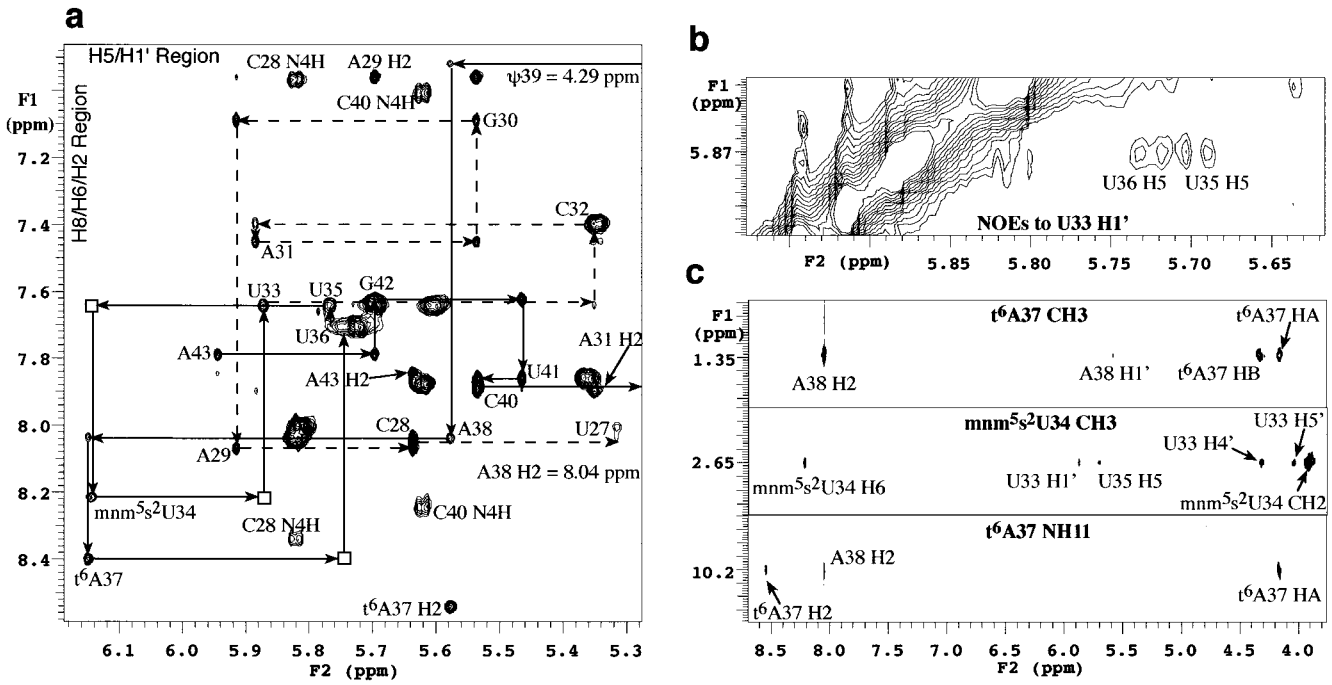

FIGURE 4: 2D NOESY NMR data of native tRNA^{Lys} ASL at 30 °C with 10 mM $MgCl_2$. (a) The base-H1′ region: peaks are labeled next to the H1′ proton. Boxes are used for peaks that are not visible at this contour level. The connectivity is traced using solid lines from A43 to U33 and dashed lines from U33 to U27, reflecting the U-turn between U33 and mnm^{5}s^{2}U34. The A31 H2 to C32 H1′ NOE is indicated on the right by a diagonal arrow. (b) The U-turn confirming NOEs: U33H1′ to U35 and U36 H5 protons. These NOEs help place the U35pU36 phosphate in proximity to the U33 imino proton. (c) NOEs defining the positions of the t^{6}A and mnm^{5}s^{2}U side chains. Each panel is labeled with the identities of the parent peaks at the chemical shifts indicated.

for these ASLs the backbone is either unrestricted or adopts a standard A-RNA conformation. The downfield shifted ^{31}P resonances move further downfield when the magnesium concentration is increased and when the temperature is decreased, indicating that the U-turn is stabilized at low temperature and by Mg^{2+}. The spectra in the absence of Mg^{2+} show downfield resonances for the native tRNA^{Lys}ASL and tRNA^{Lys}-mnm^{5}s^{2}U34,ψ39 with the greatest downfield shift seen for the native ASL in 10 mM Mg^{2+}. These molecules also show a typical, general broadening of the ^{31}P spectra when magnesium is added.

NMR Assignment and NOE Structural Restraints. The nonexchangeable protons were assigned from 2D NOESY, COSY, and TOCSY experiments on the native tRNA^{Lys} ASL and the two doubly modified tRNA^{Lys} ASLs. The comparison of the native and the two undermodified ASLs was invaluable for making unambiguous assignments, and we were also aided by additional data for tRNA^{Lys}-s^{2}U34,ψ39 (not shown) and tRNA^{Lys}-ψ39 (*1*). Sequential NOE connectivity (Figure 4, panel a) is seen from U27 to U33, and the relative NOE intensities indicate that the RNA conformation is essentially A-form throughout this region. The sugars are 3′-endo with the exception of U33, which gives a cross-peak between the U33 H1′ and H2′ protons in the 2D TOCSY spectrum. A notable AH2 to H1′ NOE is seen between A31H2 and C32 H1′ indicated by the diagonal arrow in Figure 4, panel a. On the 3′ side of the hairpin, NOE connectivity typical of a A-form geometry is seen from t^{6}A37 to A43, and the sugars on this side are all 100% 3′-endo. The 2D NOESY shows strong sequential NOEs between mnm^{5}s^{2}U34, U35, and U36, indicative of RNA A-form stacking. The NOEs for the base to H2′, H3′ protons (Supporting Information) confirm the sequential assignments, and the relative intensities show that the structure has a basically A-form geometry for the anticodon. The A-form RNA connectivity is broken between U33 and mnm^{5}s^{2}U34 at the turn, with very weak mnm^{5}s^2-U34 H6 to U33 H1′ and H2′ NOEs and no H6 to H3′ NOE. NOEs are seen between the U33 H1′ proton and the H5 protons of U35 and U36 (Figure 4, panel b), helping place the U33 imino proton within hydrogen bonding distance of the U35pU36 phosphate. The corresponding H6 to H1′ NOEs were significantly overlapped with the U35 and H36 sequential NOEs; therefore, the restraints to U33 were based on the H5-H1′ NOEs.

NOEs involving methyl groups on the hypermodified nucleosides and for the NH11 amide proton of t^{6}A37 are shown in Figure 4, panel c. The NH11 amide proton of t^{6}A has NOE connectivity to the side chain protons and to t^6-A37 H2 and A38 H2 protons. The threonyl CH_3, Hα, and Hβ protons give NOEs to A38 H2, and the CH_3 has an NOE to A38 H1′. The CH_3 of the mnm^{5}s^{2}U34 side chain also has numerous internucleotide NOEs to both U33 and U35, as well as the intranucleotide NOEs to H6 and the CH_2 group. A corresponding set of NOEs was seen for the CH_2 group and helped confirm the assignment of the methyl NOEs. The complementary NOEs for the CH_3 and CH_2 groups position the side chain in the structures and provided long-range structural information in that key region.

DISCUSSION

CD Supports a Conventional tRNA Conformation. Sulfur-modified uridine nucleosides have a long wavelength UV absorption with a maximum near 330 nm, and this contributes a band in the CD spectrum that is sensitive to local RNA structure (*17*, *37*−*39*). The sign and intensity of the sulfur CD band can be used to monitor structural stability and even to probe base pairing interactions. An unconven-

tional structure for $tRNA^{Lys}$ was first proposed based on a comparative CD study with $tRNA^{Glu}$, which also has the hypermodified mnm^5s^2U nucleoside at position 34 in the anticodon (*17*). The structure of the $tRNA^{Lys}$ anticodon was proposed to be significantly different from that of $tRNA^{Glu}$ based on a positive CD band in $tRNA^{Lys}$. This CD profile suggested that the mnm^5s^2U nucleoside was hydrogen bonded in $tRNA^{Lys}$ but not in $tRNA^{Glu}$. A critical assumption was that mnm^5s^2U34 was the only sulfur-containing nucleoside in *E. coli* $tRNA^{Lys}$. However, *E. coli* $tRNA^{Lys}$ contains 4-thiouridine (s^4U) at position 8 in addition to mnm^5s^2U34. The positive CD band at 330 nm is very characteristic of the s^4U8 nucleoside in tRNA (*37*), which forms the highly conserved reversed-Hoogsteen tertiary base pair with A14 (*40*, *41*).

The CD of our native $tRNA^{Lys}$ ASL (Figure 2, trace c) is different from that of the full-length, native $tRNA^{Lys}$ (Figure 2, trace a and reported previously) (*17*). The negative ellipticity indicates the structure of the tRNA anticodon does not contain an unconventional interaction involving mnm^5s^2-U34. Furthermore, the similar CD spectra for oxidized $tRNA^{Lys}$ and the native $tRNA^{Lys}$ ASL indicate that the ASL is an appropriate model for the $tRNA^{Lys}$ anticodon. Proposing a structural model based simply on the CD spectra is problematic as we have shown, but a negative band for the ellipticity from mnm^5s^2U is consistent with a single-stranded environment.

Secondary Structure and Stability. The downfield, imino proton NMR spectra in Figure 3 indicate that the native ASL and the two doubly modified ASLs form stable stem-loop structures. Slowly exchanging imino proton resonances are seen for the three internal Watson−Crick base pairs and for both the N3-H and N1-H imino protons of ψ39 in the A31-ψ39 base pair. Pseudouridine stabilizes each ASL, and the geometry of the A-ψ base pair and stacking stabilization on the 3′ side of the anticodon loop is similar to that of the $tRNA^{Lys}$-ψ39 ASL (*1*). The mnm^5s^2U34 modification has little effect on the imino spectrum and increases the thermodynamic stability by only 1.4 °C. While this effect is modest, we saw no change in the thermodynamic stability for $tRNA^{Lys}$ ASLs with the simple s^2U34 modification. The effects of s^2U without the side chain are complicated by a noticeable change in the nucleoside dynamics. The s^2U34 H1′ proton is significantly broadened in this ASL, and we also saw that the H5 protons of the loop uridines are broadened as was reported previously by Agris and co-workers (*2*). We found that the $tRNA^{Lys}$-s^2U34 ASL NMR spectrum is further complicated by duplex formation above approximately 300 μM concentration; however, the introduction of ψ39 in the $tRNA^{Lys}$-s^2U34, ψ39 ASL prevented duplex formation even at concentrations above 1 mM.

The t^6A modification destabilizes the ASL by about 2 °C and also diminishes the stabilizing effect of ψ39. It appears that the conformational effects of t^6A that promote a nativelike anticodon structure place stress on the A31-ψ39 base pair, resulting in destabilization of the stem. Another perspective that we believe is useful for interpreting this effect is that the native structure introduces conformational stress on the upper loop/lower stem region, and this in turn explains why the compensating effects of ψ39 modification are needed. The critical function of t^6A is to adjust the stacking geometry between 36 and 37 and to promote a conformation in the upper loop that allows for the U33 N3-H to 35p36 hydrogen bond (Figure 6). This interaction is a classic structural feature of the U-turn geometry and demonstrates that the $tRNA^{Lys}$ anticodon adopts a conventional $tRNA^{Phe}$-like conformation (Figure 5). The U33 N3-H imino resonance and a downfield shifted ^{31}P resonance for the 33p34 phosphate are the two characteristic NMR signatures of U-turns (*43*, *44*, *46*).

Structural Environment of the Modified Nucleosides. Substantial stabilization of the anticodon loop structure occurs upon introduction of the modified nucleosides at positions 34 and 37. We have previously shown that the unmodified and ψ39-containing $tRNA^{Lys}$ ASLs are very dynamic with only weak stacking between U35-U36 and no NOEs to indicate base stacking between U34 and U35 (*1*). The ^{31}P NMR spectrum of the native ASL has a single phosphorus resonance shifted significantly downfield of the envelope of resonances (*20*). This resonance was assigned to the 33p34 phosphate using 2D ^1H-^{31}P COSY and ^1H-^{31}P hetero-TOCSY-TOCSY experiments. The significant shift in the ^{31}P NMR spectrum indicates either the α or ζ angle is trans, consistent with a π-turn geometry in the tRNA ASL (*44*, *45*). We also observed a downfield shifted 33p34 phosphorus resonance for $tRNA^{Lys}$-mnm^5s^2U34,ψ39 (Supporting Information), indicating the phosphate backbone angle is also trans in the doubly modified ASL. In contrast, we saw no such NMR resonance for $tRNA^{Lys}$-s^2U34,ψ39 or $tRNA^{Lys}$-t^6A37,ψ39, indicating that for these ASLs the backbone is either unrestricted or adopts a standard A-RNA conformation. We believe that the additional conformational restriction is a simple result of steric restraints imposed by the mnm^5 side chain, but an ionic interaction between the amine and the turning phosphate could also help position the wobble nucleoside. Preliminary data from our laboratory on mcm^5s^2U, the eukaryotic modification in human $tRNA^{Lys,3}$, indicate that the structural effects are similar for the two hypermodified wobble nucleosides although the pattern of hydrogen bond donors/acceptors in the side chains is quite different. We think this also argues in favor of a steric role for the side chain. The position of the mnm^5s^2U side chain is well-defined by NOEs from the CH_2 and CH_3 of the side chain to sugar protons on U33 and to the H5 proton of U35 (Figure 6).

Previous studies have shown that an ASL with s^2U34 has significant ribosome binding activity (*2*). However, our NMR data indicate that there is a substantial structural difference between the ASL with only s^2U34 and the fully modified tRNA. The introduction of the methylaminomethyl side chain causes a significant structural change; there is no indication of a U-turn for the s^2U34 modified ASL. The ribosome binding experiments compared P-site tRNA binding affinities on poly(A) and poly(AG) mRNAs. This leaves open the possibility that the native $tRNA^{Lys}$ and partially modified tRNAs will show greater affinity differences at the ribosomal A-site, which is known to be the critical step for tRNA discrimination (*47*).

The t^6A side chain is oriented distal to the base imidazole ring as seen in the crystal structure of the nucleoside (*48*) and NOEs from NH11 to the t^6A H2 proton place NH11 within hydrogen bonding distance of t^6A37 N1. There are a large number of NOEs that define the conformation of the side chain, key NOEs defining the orientation of the side

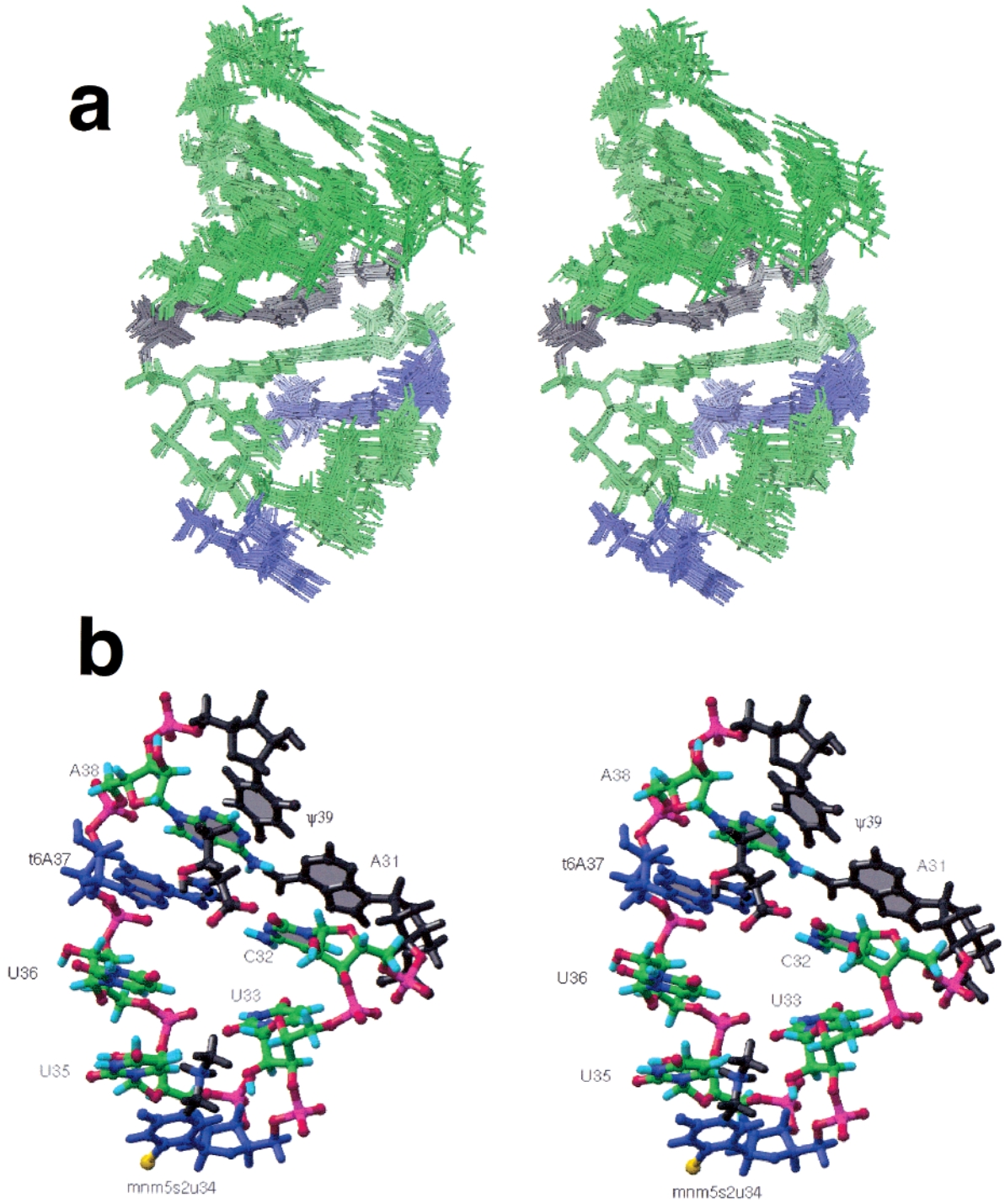

FIGURE 5: (a) Superposition of the 20 lowest energy NMR structures. The A31-ψ39 base pair is black, and mnm^{5}s^{2}U34 and t^{6}A37 are blue. (b) Structure for residues 31−39 with the base color scheme of panel a, except the modified side chain carbons and hydrogens are black, the nitrogens are blue, and the oxygens are red. Three-dimensional structural figures were made with RIBBONS (*64*).

chain relative to the base, and sequential NOEs that allow the t^{6}A nucleoside to be accurately positioned in the structure (Figure 7). No NOEs are seen from the CH_3 group of the t^{6}A side chain to the mnm^{5}s^{2}U side chain. The stable interaction between U33 N3-H and the U35pU36 phosphate is a specific result of t^{6}A modification since a slowly exchanging imino proton at 11.5 ppm was also seen for the tRNA^{Lys} ASL that contains only ψ39 and t^{6}A37 (Figure 3). Although we see no specific hydrogen bonds between functional groups on t^{6}A and neighboring nucleosides, the modification clearly strengthens the U33 imino proton hydrogen bond to the U35pU36 phosphate. No particular phosphate geometry was imposed during the refinement; therefore, the π-turn geometry results entirely from the experimental NOE restraints. It appears that avoiding an unfavorable interaction between U33 O2 and the t^{6}A amide oxygen increases helical twist, pushing the 35p36 phosphate toward the U33 imino proton. Westhof and co-workers have documented how the known tRNA anticodon structures are significantly overwound as compared to A-form RNA and have discussed the restrictions this places on the allowed sequence combinations (*49*). The t^{6}A37 modification in tRNA^{Lys} changes the unmodified ASL from a quite flexible structure into a structure having a well-stacked anticodon

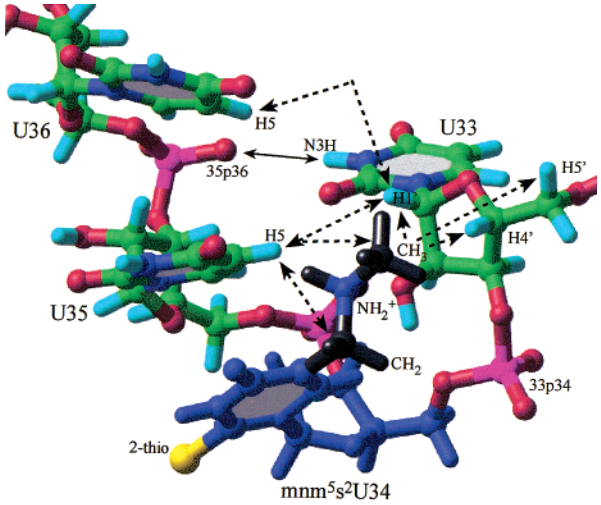

FIGURE 6: Details of the U-turn structure and mnm^{5}s^{2}U34: The key NOEs observed are indicated by dashed lines. The U33N3H−phosphate hydrogen bond is indicated with a solid arrow.

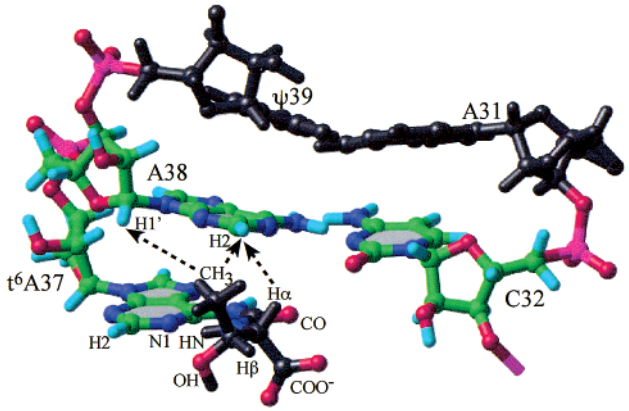

FIGURE 7: Details of t^{6}A 37, A38, ψ39, A31, and C32. Some of the key NOEs used to define the position of the t^{6}A side chain are indicated.

with a U33 imino to 35p36 phosphate hydrogen bond. The structural strain from t^{6}A37 decreases the T_m by 2 °C, but this is compensated for by an almost equal increase from mnm^{5}s^{2}U34 and a further increase in stability from ψ39.

Correction of Previous Assignments. The NMR assignments and structural interactions in our tRNA^{Lys} ASL differ significantly from that reported previously for a modified pentamer oligonucleotide (*18*). While we were not surprised that the structures differ, we found that some of our chemical shift assignments for the hypermodified nucleosides differed from those reported, and our assignments for intranucleotide NOEs contradicted those for the pentamer. We discovered that the 2D NOESY spectrum presented by Agris et al. (*18*) (their Figure 4) incorrectly assigned cross-peaks as due to internucleotide NOEs between mnm^{5}s^{2}U-34 and t^{6}A-37 when these peaks are in fact intranucleotide NOEs. The peak assigned to mnm^{5}s^{2}U34 H1′/t^{6}A37 H8 is instead an NOE from t^{6}A-37 H8 to t^{6}A H1′, and the peak assigned to t^{6}A37 H5′/mnm^{5}s^{2}U34 H6 is clearly the intrabase NOE between mnm^{5}s^{2}U34 H6 and the CH_2 group of the mnm^5 side-chain. The unambiguous data supporting the correct assignments are provided by the two doubly modified ASLs (Supporting Information) where only one of the hypermodified nucleosides is present, yet NOEs similar to those incorrectly assigned in the pentamer are still observed. The lack of long-range NOEs in the pentamer, and few sequential base to H2′ or H3′ NOEs, indicates that this molecule adopts an extended conformation in solution.

Table 1: Structural Statistics

no. structures used/calculated	20/35
distance restraints	
measured	123
lower and upper bounds	102
base pair restraints	15
dihedral restraints	161
chiral restraints	68
distance violations	none > 0.45 Å
dihedral violations	none > 10°
average pairwise RMSDs as compared to the average structure (Å)	
for all atoms	0.52 ± 0.16
stem	0.45 ± 0.16
loop	0.53 ± 0.11
anticodon	0.62 ± 0.02
average distances for key interactions (Å)	
U33 N3H to 35p36 oxygen	2.30 ± 0.36 (1.79)[a]
ψ39 N1H to p39 oxygen	4.51 ± 0.03 (4.04)[a]
ψ39 N1H to p38 oxygen	5.07 ± 0.22 (5.90)[a]
A31H2 to C32 H1′	4.23 ± 0.06 (4.29)[a]

[a] Distances for tRNAPhe from Rhodes and co-workers (*51*) in parentheses.

Comparison of tRNA^{Lys} with Yeast tRNA^{Phe}. The tRNA^{Lys} structure is generally similar to the early tRNA^{Phe} crystal structure (*50*), but a comparison of the upper loop region and the anticodon gives some insight into the degree to which certain tRNA structural elements are conserved. First, the A31H2 to C32H1′ distance is 5.3 Å in the 2.5-Å crystal structure as compared to 4.1 Å in the tRNA^{Lys} structure, resulting in different angles between the stem and the loop. Interestingly, in the recently refined 2.0-Å tRNA^{Phe} crystal structure (*51*), this distance is decreased dramatically to 4.29 Å. The strong H2 to H1′ NOE (Figure 4, panel a) we observe between A31 and C32 is typical for A-form stacking. This NOE was seen in all the partially modified tRNA^{Lys} ASLs in solution and in unrelated ASLs of tRNA^{Leu} that also have A31 (Durant and Davis, unpublished). The structure in this region may be important for understanding the "extended anticodon" hypothesis of Yarus, which describes how the identities of the last two stem base pairs and the upper loop affect the function of the anticodon (*52*). The identity of tRNA isoacceptors is of course characterized by the anticodon sequence, but this in turn places specific restrictions on the sequence of the upper loop and the last two base pairs of the stem. This hypothesis was tested by functional analysis of tRNAs with unnatural combinations within the extended anticodon (*52*) and recently discussed in a detailed structural context by Auffinger and Westhof (*49*). The structural similarity between tRNA^{Lys} and the recent tRNA^{Phe} structure (*51*) supports the hypothesis that the structure in the upper loop might be conserved.

A significant structural difference for tRNA^{Lys} as compared to tRNA^{Phe} is that there is some percentage of 2′-endo conformation for all the residues from U33 to U36 in contrast to the 100% 3′-endo residues in tRNA^{Phe}. This implies that the anticodon residues still have some conformational flexibility, consistent with the still relatively weak U33 imino peak. Of the anticodon residues, the mnm^{5}s^{2}U34 wobble nucleoside has the lowest percentage of 2′-endo conformation (<30%) as expected from the strong effect sulfur has on

nucleoside conformation (*53*, *54*), but U36 is approximately 50% 2′-endo despite being adjacent to t^{6}A37, which is 100% 3′-endo. While it is often stated that the 3′ side of the anticodon in tRNA^{Phe} forms a continuous stack, in fact the base stacking is quite discontinuous between 36 and 37. The tRNA^{Lys} structure exhibits this characteristic as well. There is a marked difference between the sugar conformation for U36 and t^{6}A37, but in the tRNA^{Phe} structure all the anticodon (purine) nucleotides are 3′-endo in the crystal structure as well as in solution (*43*). Nevertheless, both the t^{6}A37 modification in tRNA^{Lys} and yW37 in tRNA^{Phe} promote a stacking arrangement that is similar, with the hypermodified purine residue positioned to stack over the helix formed by the codon−anticodon complex rather than stacking directly on the third anticodon nucleotide (*55*, *56*). The hypermodified nucleosides at position 37 in the two tRNAs also have the role of preventing a closed anticodon loop structure (*1*, *57*).

CONCLUSIONS

The structure described here allows us to correct several misconceptions regarding tRNA structure and function. Studies of wobble pairing, frameshifting, or miscoding invariably invoke the potential for unusual structures to explain the unexpected tRNA behavior. This has been especially true of *E. coli* tRNA^{Lys} since modifications have a dramatic effect on coding (*13*). Programmed −1 frameshifts in *E. coli* depend on the preference for AAA Watson−Crick pairing over AAG wherein the thiolated wobble nucleoside promotes slippage from G to A (*12*, *15*). The effect of the wobble modification on misreading of asparagine codons (AAU/C) has been investigated, and the results were confusing in the context of previous models (*16*). The mnm^{5}U34 mutant had decreased misreading, while it was hypothesized that this tRNA should have increased wobble, therefore more misreading of the noncognate codon. However, the codon−anticodon interaction in the mnm^{5}U34 containing tRNA lacks the stabilizing effects that the 2-thio would contribute to neighboring A−U interactions involving U35 and U36 (*58*). One could imagine then that the more disordered tRNA^{Lys} mnm^{5}U34 binds the asparagine codon poorly, while the more ordered tRNA^{Lys}-mnm^{5}s^{2}U34 forms a stronger interaction at U35 and U36, which more than compensates for the poor geometry of the wobble U−U and U−C pairs (*59*). Thermodynamic measurements for U−U and U−C pairs show they provide half the stabilization of a canonical A−U pair, but the enthalpy for these interactions is still quite favorable (*60*). The high level of misreading by the native tRNA^{Lys} can be explained by mnm^{5}s^{2}U stabilization of two out of three reading (*61*) and the lack of significant unfavorable interactions between the wobble base and the third codon nucleotide.

The structure of the tRNA^{Lys} ASL explains the preference for A over G simply by the thermodynamic stabilization of A−s^{2}U as compared to G−s^{2}U (*62*). A G−s^{2}U wobble pair is simply less stable than an A−s^{2}U Watson−Crick pair. The effect of the mnm^5 modification is likewise explained since the side chain modification restricts the conformational freedom of the wobble base and promotes a canonical, tRNA^{Phe}-like conformation. The U-turn structure of tRNA^{Lys} holds the wobble nucleoside in a relatively rigid, nearly A-RNA conformation that in turn helps stabilize stacking with U35 and U36. Nucleoside modifications that promote a rigid loop conformation are particularly important for tRNA^{Lys} function since the codon−anticodon interaction is mediated by three relatively weak uridine-containing base pairs (*63*). Preorganization is necessary in tRNA^{Lys} to reduce the entropic cost for the formation of A−U base pairs that have relatively modest levels of enthalpic stabilization (*60*). The anticodon interaction with the HIV-1 A rich loop (*5*) is presumably stabilized for the same reason that modification is required for stable codon−anticodon interaction, a preorganized tRNA and favorable Watson−Crick pairing stabilized by a sulfur-modified nucleoside. The mnm^{5}s^{2}U nucleoside promotes an A-RNA conformation for the wobble nucleoside, stabilizes stacking of the anticodon nucleosides, and stabilizes the π-turn phosphate conformation. The hypermodified t^{6}A nucleoside promotes a base-stacking conformation in the upper loop that positions the 35p36 phosphate for hydrogen bonding with U33 and further stabilizes the U-turn. The modification pattern in tRNA$^{Lys}_{UUU}$ is evolutionarily conserved and represents an elaborate, but apparently required, mechanism for stabilizing the tRNA anticodon structure.

ACKNOWLEDGMENT

We thank John Atkins and Ray Gesteland for educating us about translation, and Steve Alam, Jim McCloskey, and Wes Sundquist for comments on the manuscript.

SUPPORTING INFORMATION AVAILABLE

^{31}P NMR spectra, base-H1′ NOESY assignment walks, and base-sugar NOESY expansions for fully modified and doubly modified tRNA^{Lys} ASLs. This material is available free of charge via the Internet at http://pubs.acs.org.

REFERENCES

1. Durant, P. C., and Davis, D. R. (1999) *J. Mol. Biol. 285*, 115−131.
2. Ashraf, S., Sochacka, E., Cain, R., Guenther, R., Malkiewicz, A., and Agris, P. (1999) *RNA 5*, 188−194.
3. Von Ahsen, U., Green, R., Schroeder, R., and Noller, H. (1997) *RNA 3*, 49−56.
4. Tamura, K., Himeno, H., Asahara, H., Hasegawa, T., and Shimizu, M. (1992) *Nucleic Acids Res. 20*, 2335−2339.
5. Isel, C., Westhof, E., Massire, C., Le Grice, S. F. J., Ehresmann, B., Ehresmann, C., and Marquet, R. (1999) *EMBO J. 18*, 1038−1048.
6. Zhang, Z., Kang, S., Li, Y., and Morrow, C. (1998) *RNA 4*, 394−406.
7. Barat, C., le Grice, S. F. J., and Darlix, J.-L. (1991) *Nucleic Acids Res. 19*, 751−757.
8. Essink, B. B. O., Das, A. T., and Berkhout, B. (1995) *J. Biol. Chem. 270*, 23867−23874.
9. Huang, Y., Shalom, A., Li, Z., Wang, J., Mak, J., Wainberg, M. A., and Kleiman, L. (1996) *J. Virol. 70*, 4700−4706.
10. Isel, C., Marquet, R., Keith, G., Ehresmann, C., and Ehresmann, B. (1993) *J. Biol. Chem. 268*, 25269−25272.
11. Isel, C., Lanchy, J.-M., Le Grice, S. F. J., Ehresmann, C., Ehresmann, B., and Marquet, R. (1996) *EMBO J. 15*, 917−924.
12. Tsuchihashi, Z., and Brown, P. (1992) *Genes Dev. 6*, 511−516.
13. Atkins, J. F., Herr, A. J., Massire, C., O'Connor, M., Ivanov, I., and Gesteland, R. F. (2000) in *The Ribosome: Structure, Function, Antibiotics, and Cellular Interaction* (Garrett, R. A., Douthwaite, S. R., Liljas, A., Matheson, A. T., Moore, P. B., and Noller, H. F., Eds.) pp 369−383, ASM Press, Washington, DC.

14. Mejlhede, N., Atkins, J., and Neuhard, J. (1999) *J. Bacteriol. 181*, 2930−2937.
15. Brierley, I., Meredith, M. R., Bloys, A. J., and Hagervall, T. G. (1997) *J. Mol. Biol. 270*, 360−373.
16. Hagervall, T. G., Pomerantz, S. C., and McCloskey, J. A. (1998) *J. Mol. Biol. 284*, 33−42.
17. Watanabe, K., Hayashi, N., Oyama, A., Nishikawa, K., Ueda, T., and Miura, K. (1994) *Nucleic Acids Res. 22*, 79−87.
18. Agris, P. F., Guenther, R., Ingram, P. C., Basti, M. M., Stuart, J. W., Sochacka, E., and Malkiewicz, A. (1997) *RNA 3*, 420−428.
19. Cate, J. H., Yusupov, M. M., Yusupova, G. Z., Earnest, T. N., and Noller, H. F. (1999) *Science 285*, 2095−2104.
20. Sundaram, M., Crain, P. F., and Davis, D. R. (2000) *J. Org. Chem. 65*, 5609−5614.
21. Damha, M. J., and Ogilvie, K. K. (1993) *Methods Mol. Biol. 20*, 81−114.
22. Gasparutto, D., Livache, T., Bazin, H., Dupla, A., Guy, A., Khordin, A., Molko, D., Roget, A., and Teoule, R. (1992) *Nucleic Acids Res. 20*, 5159−5166.
23. Wincott, F., DiRenzo, A., Shaffer, C., Grimm, S., Tracz, D., Workman, C., Sweedler, D., Gonzalez, C., Scaringe, S., and Usman, N. (1995) *Nucleic Acids Res. 23*, 2677−2684.
24. Pomerantz, S. C., and McCloskey, J. A. (1990) *Methods Enzymol. 193*, 796−824.
25. Crain, P. F. (1990) *Methods Enzymol. 193*, 782−790.
26. Laing, L. G., and Draper, D. E. (1994) *J. Mol. Biol. 237*, 560−576.
27. Lapham, J., Rife, J. P., Moore, P. B., and Crothers, D. M. (1997) *J. Biomol. NMR 10*, 255−262.
28. Jeener, J., Meier, B. H., Bachmann, P., and Ernst, R. R. (1979) *J. Chem. Phys. 71*, 4546−4553.
29. Levitt, M., Freeman, R., and Frenkel, T. (1982) *J. Magn. Reson. 47*, 328−330.
30. Varani, G., and Tinoco, I. (1991) *Q. Rev. Biophys. 24*, 479−532.
31. Mori, S., Abeygunawardana, C., O'Neil Johnson, M., and van Zul, P. C. M. (1995) *J. Magn. Reson. Series B 108*, 94−98.
32. Sklenar, V., and Bax, A. (1987) *J. Am. Chem. Soc. 109*, 7525−7526.
33. Kellogg, G. W. (1992) *J. Magn. Reson. 98*, 176−182.
34. Piantini, U., Sorenson, A. W., and Ernst, R. R. (1982) *J. Am. Chem. Soc. 104*, 6800−6801.
35. Rife, J. P., Stallings, S. C., Correll, C. C., Dallas, A., Steitz, T. A., and Moore, P. B. (1999) *Biophys. J. 76*, 65−75.
36. Cornell, W. D., Cieplak, P., Bayly, C. I., Gould, I. R., Merz, K. M., Ferguson, D. M., Spellmeyer, D. C., Fox, T., Caldwell, J. W., and Kollman, P. A. (1995) *J. Am. Chem. Soc. 117*, 5179−5197.
37. Scott, J. F., and Schofield, P. (1969) *Proc. Natl. Acad. Sci. U.S.A. 64*, 931−938.
38. Watanabe, K., Oshima, T., and Nishimura, S. (1976) *Nucleic Acids Res. 3*, 1703−1713.
39. Willick, G., Oikawa, K., and Kay, C. M. (1973) *Biochemistry 12*, 899−904.
40. Wong, K. L., and Kearns, D. R. (1974) *Nature 252*, 738−739.
41. Davis, D. R., Griffey, R. H., Yamaizumi, Z., Nishimura, S., and Poulter, C. D. (1986) *J. Biol. Chem. 261*, 3584−3587.
42. Griffey, R. H., Poulter, C. D., Yamaizumi, Z., Nishimura, S., and Hawkins, B. H. (1983) *J. Am. Chem. Soc. 105*, 143−145.
43. Clore, G., Gronenborn, A., Piper, E., McLaughlin, L., Graeser, E., and Van Boom, J. (1984) *Biochem J. 221*, 737−751.
44. Schweisguth, D., and Moore, P. (1997) *J. Mol. Biol. 267*, 505−519.
45. Saenger, W. (1984) *Principles of Nucleic Acid Structure*, Springer-Verlag, New York.
46. Jucker, F. M., and Pardi, A. (1995) *RNA 1*, 219−222.
47. Yarus, M., and Smith, D. (1995) in *tRNA: Structure, Biosynthesis, and Function* (Soll, D., and RajBhandary, U., Eds.) pp 443−469, ASM Press, Washington, DC.
48. Parthasarathy, R., Ohri, J., and Chheda, G. (1977) *Biochemistry 16*, 4999−5007.
49. Auffinger, P., and Westhof, E. (1999) *J. Mol. Biol. 292*, 467−483.
50. Jack, A., Ladner, J. E., and Klug, A. (1976) *J. Mol. Biol. 108*, 619−649.
51. Jovine, L., Djordjevic, S., and Rhodes, D. (2000) *J. Mol. Biol. 301*, 401−414.
52. Yarus, M. (1982) *Science 218*, 646−652.
53. Yokoyama, S., Watanabe, T., Murao, K., Ishikura, H., Yamaizumi, Z., Nishimura, S., and Miyazawa, T. (1985) *Proc. Natl. Acad. Sci. U.S.A. 82*, 4905−4509.
54. Sierzputowska-Gracz, H., Sochacka, E., Malkiewicz, A., Kuo, K., Gehrke, C., and Agris, P. (1987) *J. Am. Chem. Soc. 109*, 7171−7177.
55. Fuller, W., and Hodgson, A. (1967) *Nature 215*, 817−821.
56. Grosjean, H., Soll, D. G., and Crothers, D. M. (1976) *J. Mol. Biol. 103*, 499−519.
57. Basti, M., Stuart, J., Lam, A., Guenther, R., and Agris, P. (1996) *Nature Struct. Biol. 3*, 38−44.
58. Kumar, R. K., and Davis, D. R. (1997) *Nucleic Acids Res. 25*, 1272−1280.
59. Lim, V. (1994) *J. Mol. Biol. 240*, 8−19.
60. Serra, M. J., Turner, D. H., and Freier, S. M. (1995) *Methods Enzymol. 259*, 243−261.
61. Lustig, F., Elias, P., Axberg, T., Samuelsson, T., Tittawella, I., and Lagerkvis, U. (1981) *J. Biol. Chem. 256*, 2635−2643.
62. Testa, S. M., Disney, M. D., Turner, D. H., and Kierzek, R. (1999) *Biochemistry 38*, 16655−16662.
63. Grosjean, H., and Chantrenne, H. (1980) in *Molecular Biology Biochemistry and Biophysics* (Chaperville, F., and Haenni, A., Eds.) pp 347−367, Springer-Verlag, Berlin.
64. Carson, M. (1991) *J. Appl. Crystallogr. 24*, 958−961.

BI0014655